Ultrafast Dynamics of Metal Plasmons Induced by 2D Semiconductor Excitons in Hybrid Nanostructure Arrays

Abdelaziz Boulesbaa[1,], Viktoriia E. Babicheva[2], Kai Wang[1], Ivan I. Kravchenko[1], Ming-Wei Lin[1], Masoud Mahjouri-Samani[1], Christopher Jacob[1], Alexander A. Puretzky[1], Kai Xiao[1], Ilia Ivanov[1], Christopher M. Rouleau[1], and David B. Geohegan[1]*

[1]Center for Nanophase Materials Sciences, Oak Ridge National Laboratory, Oak Ridge, TN 37831, USA

[2]Center for Nano-Optics, Georgia State University, P.O. Box 3965, Atlanta, GA 30302, USA

*Address correspondence to boulesbaaa@ornl.gov

With the advanced progress achieved in the field of nanotechnology, localized surface plasmons resonances (LSPRs) are actively considered to improve the efficiency of metal-based photocatalysis, photodetection, and photovoltaics. Here, we report on the exchange of energy and electric charges in a hybrid composed of a two-dimensional tungsten disulfide (2D-WS_2) monolayer and an array of aluminum (Al) nanodisks. Femtosecond pump-probe spectroscopy results indicate that within ~830 fs after photoexcitation of the 2D-WS_2 semiconductor, energy transfer from the 2D-WS_2 excitons excites the plasmons of the Al array. Then, upon the radiative and/or nonradiative damping of these excited plasmons, energy and/or electron transfer back to the 2D-WS_2 semiconductor takes place as indicated by an increase in the reflected probe at the 2D exciton transition energies at later time-delays. This simultaneous exchange of energy and charges between the metal and the 2D-WS_2 semiconductor resulted in an extension of the average lifetime of the 2D-excitons from ~15 to ~58 ps in absence and presence of the Al array, respectively. Furthermore, the indirectly excited plasmons were found to live as long as the 2D-

WS_2 excitons exist. The demonstrated ability to generate exciton-plasmons coupling in a hybrid nanostructure may open new opportunities for optoelectronic applications such as plasmonic-based photodetection and photocatalysis.

Localized surface plasmons resonances (LSPRs) are collective oscillations of surface conduction electrons in metal nanoparticles. Due to their strong dependence on the shape and size of the particle, the light-matter interaction at the nanometer scale using these photonic modes can be tailored to specific needs. [1-5] This unique feature has made LSPRs highly useful in several application fields ranging from photocatalysis to photodetection, photovoltaics, and integrated quantum information science.[6-11] Following photoexcitation, LSPRs relax radiatively by emitting a photon or non-radiatively through the creation of hot electron–hole pairs via Landau damping on a sub-100 fs time-scale.[2,5,12,13] In most cases, LSPRs are either used for local field enhancement, and thus increasing light absorption between neighboring metal nanostructures,[4] or hot-electron transfer.[9,14] The former application has been communicated in several reports.[15-18] For example, in heterostructures involving two-dimensional transition metal dichalcogenide (2D-TMD) semiconductors and plasmonic arrays, the semiconductor photoluminescence (PL) was enhanced several times[15-18] due to local-field enhancement which led to more absorbed photons by the 2D-TMDs and consequently an enhancement in PL intensity was observed. For hot-electron transfer based applications such as photodetection and photocatalysis, the difficulty arises from the requirement that the transfer has to happen before the ultrafast relaxation of hot electrons. For example, in metal-based photodetectors where a metal is interfaced with a semiconductor forming a Schottky barrier,[6] in order to have a photocurrent, hot electrons resulting from Landau-damping of LSPRs have to reach the conduction band of the semiconductor before these electrons are dissipated. It is well established in the literature that rapidly after their formation, hot electrons undergo electron-electron scattering in the conduction band of the metal within hundreds of femtoseconds, and then electron-phonon relaxation within the following few

picoseconds.[3,19] One way to overcome this limitation is to extend the lifetime of the hot-electrons. In this letter, we demonstrate how plasmons in an aluminum (Al) array of nanodisks are indirectly excited through Förster resonance energy transfer (FRET) from photogenerated excitons of a two-dimensional tungsten disulfide (2D-WS_2) monolayer with a time-constant of ~830 fs. Ultrafast pump-probe spectroscopy indicated that the excitation of plasmons in Al continues for the long lifetime of the 2D-WS_2 excitons, providing electrons to much longer times corresponding to the lifetime of 2D-WS_2 semiconductor excitons. Additionally, the average lifetime of 2D-WS_2 excitons in the absence and presence of the Al array went from ~15 ps to ~58 ps, respectively.

2D-WS_2 monolayers were prepared following the chemical vapor deposition (CVD) procedure as previously reported.[20,21] The Al plasmonic array is formed of nanodisks of diameter D=~295 nm, height H=~45 nm, and spaced by a pitch distance (center to center) P=~420 nm (see methods in the supplementary information). Shown in **Figure 1a** is a scanning electron microscopy (SEM) image of the heterostructure that was studied. It is composed of a 2D-WS_2 monolayer partially covered with an Al plasmonic array that is a pattern of nanodisks (D ~295 nm, H ~45 nm, and P~420 nm). Measurement of the 2D-WS_2 PL on and off the plasmonic array (areas 3 and 2, respectively, in **Figure 1a**) shows that the PL intensity was doubled and blue-shifted by ~ 6 meV in the presence of the Al array (**Figure 1b**). Since the excitation energy (2.33 eV) was within the plasmonic resonances, the local electromagnetic field was strongly enhanced, and gave rise to increased optical absorption into the 2D-WS_2 monolayer, thereby enhancing the PL emission intensity.[15-17] Another scenario that may explain the enhancement of the 2D-PL is through tunneling of hot-electrons generated as a consequence of plasmons Landau damping to the conduction band of the 2D-WS_2 monolayer.[22] The boosting

of a 2D-TMD PL using plasmonics has been achieved previously for 2D molybdenum disulfide (MoS_2) monolayers.[15-17] However, the effect of excitons on plasmons can manifest in term of FRET, where excitons resonantly transfer energy to plasmons and excite them.[23] In **Figure 1c**, we illustrate the hypothesis that excitons photogenerated in the 2D-WS_2 monolayer diffuse long distances within the crystal,[24] leading to the excitation of plasmons within the Al nanodisk array through FRET.

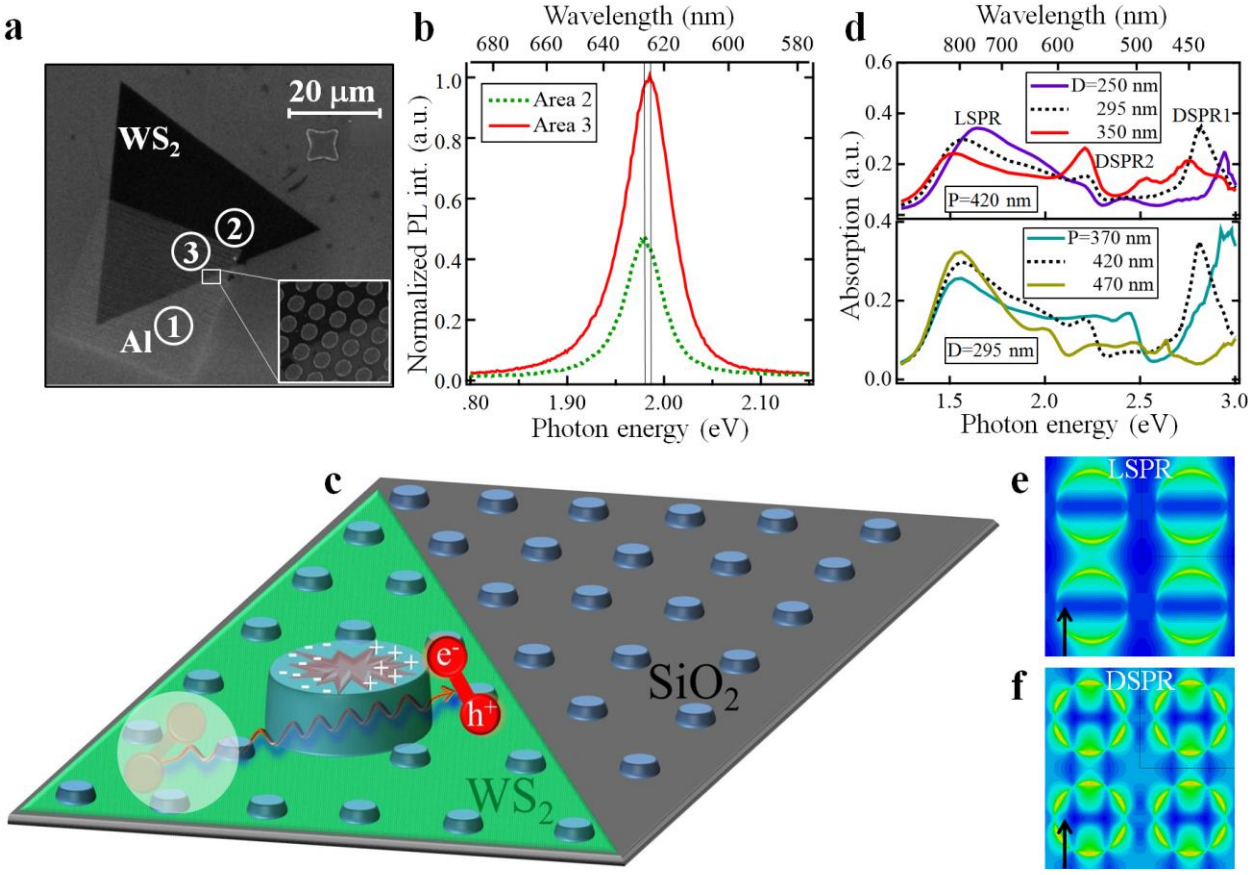

Figure 1. a. SEM image of the sample that was studied showing a 2D-WS_2 monolayer crystal (dark triangle) with a portion of it covered with a plasmonic array (bright square). The inset is a magnified image showing a portion of the array. Areas 1, 2, and 3 indicate the locations studied with ultrafast spectroscopy. **b.** 2D-WS_2 PL spectra measured from areas 2 and 3 indicated in **a**. following excitation at ~2.33 eV, showing that the 2D-PL in the presence of the plasmonic array

is enhanced by a factor of 2, and blue-shifted (note the vertical lines indicate the center of PL peaks). **c.** A schematic of the 2D-WS_2/plasmonic array heterostructure showing that while 2D-excitons propagate within the heterostructure, they transfer energy to the plasmonic modes of the array. **d.** Numerical simulations of the absorption in an infinite periodic array of nanodisks: the top panel corresponds to arrays with different diameters, *D*, and fixed pitch equal to 420 nm. The bottom panel shows absorbance for different pitches, P, and a fixed diameter equal to 295 nm. The dashed plot corresponds to the array that was studied. LSPR denotes low-energy surface plasmon resonance, and DSPR1 and DSPR2 denote high-energy resonances. **e.** and **f.** Electric field distributions 1 nm beneath the array – i.e., within the SiO_2, with the vertical black arrows indicate the field polarization. **e.** LSPR distribution at 1.6 eV. **f.** DSPR1 distribution at 2.8 eV.

Before testing this hypothesis, we first characterized the plasmonic modes of the Al array. Shown in **Figure 1d** are the calculated energy absorption spectra inside the Al nanodisks having a diameter *D*, and height *H=~45* nm, all arranged in an infinite square lattice with pitch *P*. The low-energy peak (~1.6 eV) corresponds to electric dipole excitation, assigned to localized surface plasmon resonance (LSPR, **Figure 1e**). A number of higher-multipole resonances are excited at higher energies, and they spectrally overlap with the collective lattice resonances, giving rise to delocalized surface plasmons resonances (DSPR)[25] as shown in **Figure 1f**. Note that DSPR1 corresponds to lattice resonance with $\lambda_{DSPR1} \approx P$, while DSPR2 corresponds to $\lambda_{DSPR2} \approx P \times n_{SiO2}$, where n_{SiO2} is the index of refraction of silicon dioxide. The LSPR is largely affected by changes in the nano-disk diameter (**Figure 1d**, top panel), whereas DSPR1 and DSPR2 depend strongly on the pitch of the array (bottom panel of **Figure 1d**).

Shown in **Figure 2a** is a steady-state reflection contrast spectrum measured as 100 x (R-R_0)/R_0, with R and R_0 being the intensities of reflected white light from the array (area 1 in **Figure 1a**) and from the SiO_2/Si substrate, respectively. In accordance with the calculated spectra shown in **Figure 1d**, this measured spectrum contains DSPR1, DSPR2, and LSPR features around ~2.6, ~2.1, and ~1.6 eV, respectively. Also shown in **Figure 2a** is the absorption spectrum of the 2D-WS_2 monolayer on a quartz substrate. It contains the main excitonic transition X_A, X_B, and X_C at ~2 eV, ~2.4 eV, and ~2.9 eV, respectively. Because these two spectra show a broad spectral overlap, a coupling between plasmons and excitons is expected.

One way of testing whether or not 2D-excitons excite plasmons is to selectively excite the 2D-WS_2 semiconductor to generate excitons in the hybrid system, and probe the plasmons of the Al array. Based on the steady-state spectrum of the Al array shown in **Figure 2a**, an excitation at 3.1 eV is off-resonance with respect to the resonance of plasmons. Indeed, according to **Figure 2b**, time-resolved reflectance contrast (TrR) measurements carried out on the bare Al array (region 1 in **Figure 1a**) following excitation at 3.1 eV did not contain any noticeable transient signal. Noting that in all TrR measurements, the shown signal is $\Delta R/R(\%)=100 \times (R-R_0)/R_0$, where R and R_0 are the reflected probe intensities with the pump on and off, respectively. In the case of bare 2D-WS_2 semiconductor (region 2 in **Figure 1a**), the TrR results shown in **Figure 2c** demonstrate that following the 3.1 eV excitation, two transient positive bands around ~2 eV and 2.4 eV are formed. Based on the steady-state absorption spectrum of the 2D-WS_2 monolayer shown in **Figure 2a**, these two bands represent depletions of the 2D-X_A and 2D-X_B transitions at ~2 eV and ~2.4 eV, respectively, indicating the formation of these excitons.

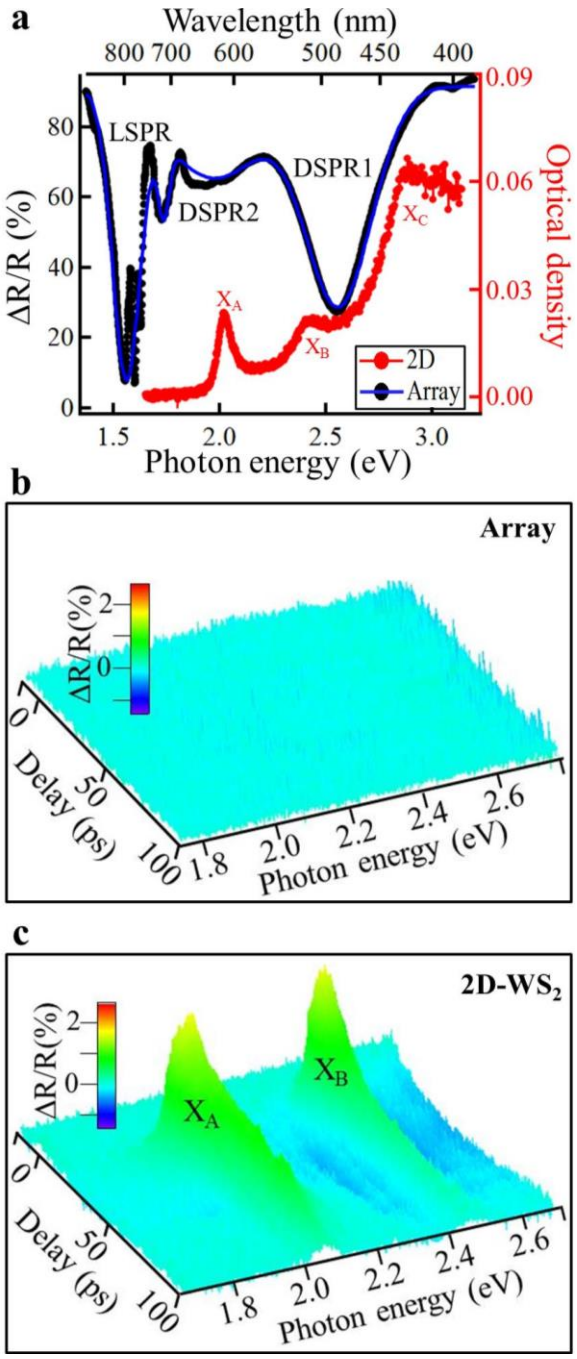

147

148 **Figure 2. a.** Measured static reflectance contrast (left y-axis) of the plasmonic array measured
149 from area 1 in **Figure 1a** (black filled circles) and the solid line is a guide for the eye. The red
150 plot is the absorption of the 2D-WS_2 monolayer on a quartz substrate plotted for reference (right
151 y-axis). It contains the main exciton transitions X_A, X_B, and X_C around ~2 eV, ~2.4 eV, and 2.9

eV, respectively. **b**. Transient reflection contrasts carried out on area 1 in **Figure 1a** (Al array) following the non-resonant excitation of plasmons at 3.1 eV. Because the excitation is off-resonance, no noticeable transient signal is observed. **c.** Transient reflection contrasts carried out on area 2 in **Figure 1a** (2D-WS_2) following excitation at 3.1 eV. Because this excitation is sufficient to generate excitons in the 2D-WS_2 monolayer, depletion of excitons X_A and X_B around ~2 and ~2.4 eV is observed.

In the case of the hybrid system of 2D-WS_2/Al array, in addition to the 2D-X_A and 2D-X_B exciton depletions, the TrR results shown in **Figure 3a** contain two additional depletions near ~2.7 eV and ~2.1 eV, corresponding to the plasmonic DSPR1 and DSPR2 modes, respectively. Because of the spectral overlap between the semiconductor and the metal signals (e.g. 2D exciton depletions, plasmons depletions, and plasmons excited state), we performed a spectral deconvolution fitting of each transient spectrum at all time-delays. To direct the simulation, we first identified the approximate centers and widths of 2D-X_A and X_B exciton depletions and the induced absorption at photon energies above ~2.55 eV based on the fit of transient spectra measured at the bare 2D-WS_2 sample. An example of the fits of transient spectra collected 500 fs time-delay for the bare 2D-WS_2 monolayer and the hybrid samples are shown in **Figure 3b** and **Figure 3c**, respectively. Additional examples of transient spectra at 5 ps, 20 ps, and 50 ps time-delays are shown in **Figure 1S** in the supplementary information. Based on steady state spectra shown in **Figure 2a**, and the transient spectrum shown in **Figure 3b**, one can easily assign the components returned by the deconvolution fit of the transient spectrum shown in **Figure 3c**. The two positive peaks in "red" represent the 2D-X_A (around ~2 eV) and 2D-X_B (around ~2.4 eV) exciton depletions, and the negative induced absorption band in "red" at photon energies higher than 2.5 eV represent the 2D-WS_2 excited state. The two positive peaks

in “blue” are depletions of DSPR1 (around ~2.7 eV) and DSPR2 (around ~2.1 eV) plasmonic modes. The negative induced absorption in “yellow” at photon energies below 2.3 eV can be assigned to the plasmons excited state.

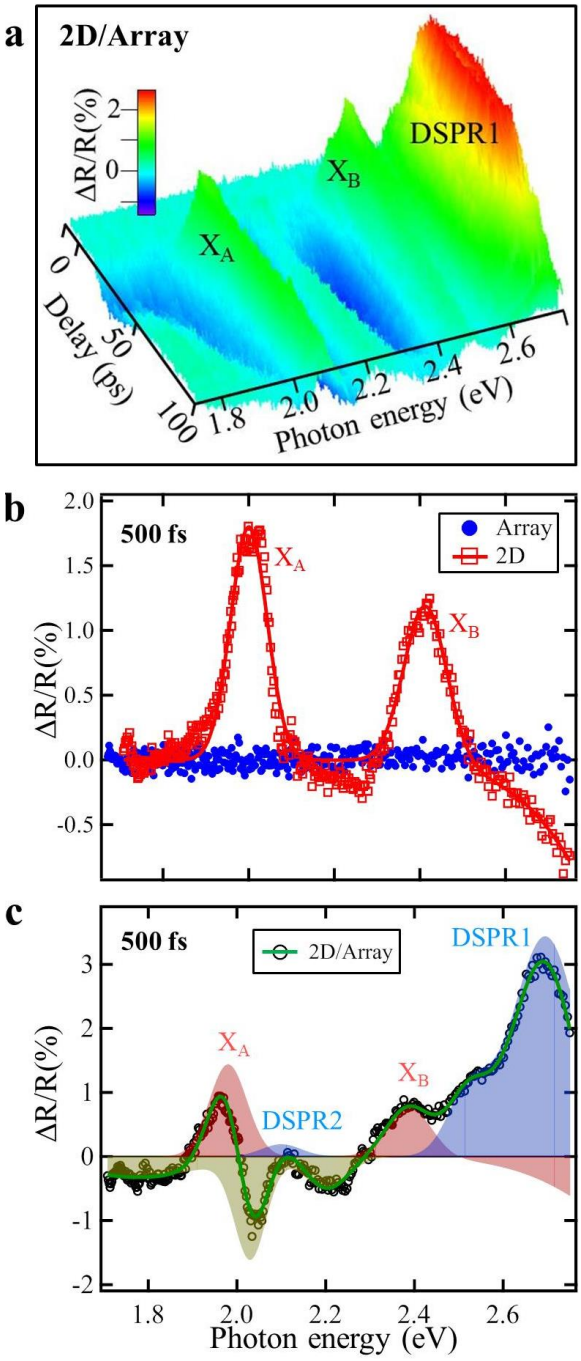

Figure 3. a. TrR from the hybrid 2D-WS_2/Al array (area 3 in **Figure 1a**) following excitation at 3.1 eV. In addition to 2D-X_A and X_B exciton depletions, the signal contains two additional

depletions near ~2.7 and ~2.1 eV, corresponding to the DSPR1 and DSPR2, respectively. **b.** Transient spectra collected at 500 fs time-delay following excitation at 3.1 eV of the 2D-WS_2 (red squares) and the Al array (blue filled circles). These spectra are cuts from **Figures** 2**b** and **2c** at 500 fs time-delay. The red solid line is a fit using a multiple-Gaussians function to extract the spectral information of 2D-X_A and 2D-X_B depletions. **c.** A spectral cut at 500 fs from Figure 3a (symbols) fit to a multiple-Gaussians function (solid line). The blue and red positive shaded areas represent the spectral components corresponding to DSPR1, DSPR2, 2D-X_A, and 2D-X_B depletions as indicated. The negative red and yellow shaded areas indicate the spectral components corresponding to the 2D-WS_2 and the metal excited state induced absorptions, respectively.

Since an excitation at 3.1 eV of the hybrid is off-resonance with respect to the plasmonic modes of the Al array (as proven in **Figure 2b**), the depletion of DSPR1 and DSPR2 observed in the presence of the excited 2D-WS_2 monolayer indicates that the photogenerated excitons in the 2D-WS_2 material excited the plasmons of the Al array, which consequently led to their depletion. Based on the spectral overlap between the plasmons modes of the Al array and the 2D-WS_2 semiconductor excitons as demonstrated in **Figure 2a**, in addition to the spatial proximity, it is likely that the 2D excitons resonantly transfer energy to the plasmonic modes of the array. We note that a FRET process has been reported for quantum dot excitons to plasmons,[23] and through this scenario of energy transfer, the depletion of DSPR1 and DSPR2 observed in **Figure 3** can be explained as follows: At photon energies corresponding to DSPR1 and DSPR2 in the probe spectrum, when the pump is off, the intensity of the reflected probe R_0, is lower due to absorption. When the pump is on, 2D excitons are generated, and if they transfer energy to the Al array and excite plasmons, the arriving probe pulse does not get absorbed because DSPR1 and

DSPR2 are already excited. Consequently, the reflected probe intensity *R,* is higher, and consequently $\Delta R/R(\%)=100 \times (R-R_0)/R_0$ is positive.

To further understand the exciton-plasmon interaction, we fitted the bleach dynamics of the 2D-X_A exciton and DSPR1 plasmons are shown in **Figure 4**. The parameters returned by the converged fits are listed in **Table 1**. In the case of bare 2D-WS_2 semiconductor sample, the 2D-X_A exciton depletion formation was instantaneous (within the instrument response function, IRF), and the decay dynamics are well described with a bi-exponential decay function. About half of the population decays with a time-constant of ~500 fs while the other half decays with a time constant of 32 ps. It has been reported in the literature that in 2D-TMDs, the sub- to few-picosecond decay is due to non-radiative recombination through Auger-type scattering and defect-assisted relaxations, and the slower decay component is due to radiative electron-hole recombination.[26,27] Based on the average exciton lifetime; τ~15 ps (see **Table 1**), and the reported exciton diffusion constant in 2D-WS_2 monolayers; D~60 cm^2/s,[28] one can estimate the exciton diffusion length $L=(D\times\tau)^{1/2}$,[24] to be on the order of ~300 nm. This suggests that the exciton drift velocity is on the order of 10^4 m/s, which is not far from the ballistic exciton transport. In the case of the hybrid sample, the 2D-X_A exciton bleach formation was slower than the IRF, and exhibit an exponential growth with a time constant of ~130 fs. Furthermore, there are two noticeable features: 1) the amplitude of the signal at early time-delays (<500 fs) is reduced, which is due to the ultrafast quenching of the signal and 2) the first decay component is slower compared to the case of bare 2D-WS_2 semiconductor, it went from ~0.5 to ~2.7 ps and the second component was more than doubled, it went from ~32 to ~71 ps. A similar comparison of the dynamics of 2D-X_B in presence and absence of the Al array are shown in **Figure S2** in the supplementary material. The quenching of the 2D-WS_2 bleach amplitude at

early time delays (<~500 fs) can be a consequence of either energy transfer or charge transfer to the Al array. However, since the bleach amplitude at later time-delays compared to the case of bare 2D-WS_2 monolayer, one can exclude the charge transfer scenario because in that case the Al array would be reduced (electron transfer) or oxidized (hole transfer) without exciting the plasmons, which can transfer energy and/or charges back to the 2D-WS_2 monolayer increasing their bleach amplitude. Consequently, we conclude that energy transfer from the 2D-WS_2 to the Al array is the most likely scenario.

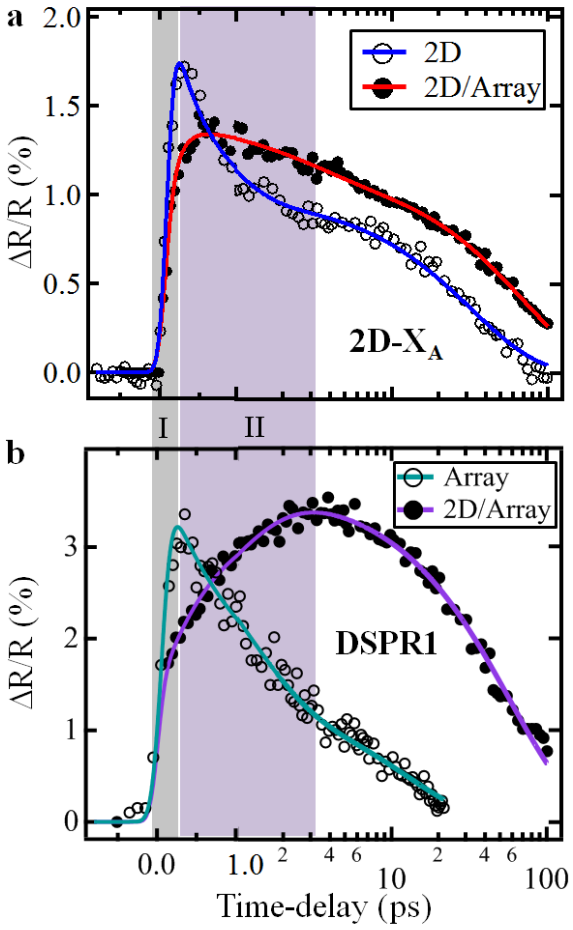

Figure 4. **a.** 2D-X_A exciton bleach dynamics in the absence (open circles) and presence of the Al plasmonic array (filled circles) following excitation at 3.1 eV. The plotted dynamics are the amplitudes of the 2D-X_A depletion signal at ~2 eV. In the case of 2D/Array sample, the

amplitudes are those of 2D-X_A peak at ~ 2 eV returned by the deconvolution fits of transient spectra as shown in **Figure 3c**. Line plots are fits using exponential functions convoluted with a Gaussian laser pulse with 45 fs duration. **b.** The open circles plot is the bleach dynamics of the DSPR1 mode following excitation at 2.6 eV and probe at 2.5 eV in the Al array without the 2D-WS_2 monolayer. The solid line is the fit to a bi-exponential decay function convoluted with a Gaussian laser pulse with 45 fs duration. Filled circles plot is the bleach dynamics of the DSPR1 mode following 3.1 eV excitation of the hybrid heterostructure. The plotted dynamics are the amplitudes of DSPR1 peak at ~2.7 eV returned by the deconvolution fits of transient spectra as shown in **Figure 3c**. The solid line is the fit to a function composed of one rise and one decay exponential components convoluted with a Gaussian laser pulse with 45 fs duration. In both **a** and **b** the time-delay axis up to 1 ps is linear while thereafter it is logarithmic. The vertical shaded areas I, and II correspond to time-delay ranges until the 2D-X_A (in absence of the Al array) and DSPR1 (in the hybrid sample) bleach signals reach their maximum amplitudes, respectively.

For the DSPR1 plasmons dynamics shown in **Figure 4b**, in the case of bare Al array without the 2D-WS_2 monolayer, the bleach formation was instantaneous and within the IRF, then it decayed rapidly with an average lifetime of ~5.3 ps (see **Table 1**), which is in agreement with the reported lifetime of hot-electrons in metals.[19] In the hybrid sample however, the growth of the signal is slower than the IRF, which is expected since plasmons are not directly excited by the laser pump, but through energy transfer from the 2D-WS_2 excitons. Therefore, the signal formation time represents the time of energy transfer from the 2D-WS_2 to the Al metal array. The fitting of these dynamics required an exponential growth component with a time constant of ~830 fs, which is the FRET time, and a decay component with a time constant of ~53 ps (see

Table 1). This lifetime is similar to that of the 2D-X_A in the hybrid sample, indicating that the electrons resulting from Landau damping of plasmons live as long as the 2D-WS_2 excitons exist.

Table 1. List of parameters obtained from fitting the 2D-X_A exciton and DSPR1 plasmons depletion dynamics in the 2D-WS_2 monolayer with and without the Al array to a bi-exponential function $F(t) = \left(\sum_i A_i e^{-t/T_i}\right)$ convoluted with a 45 fs Gaussian shaped laser pulse. In the case of the hybrid system, an additional exponential growth component $Be^{-t/k}$ was added to $F(t)$ to describe the slow growth of 2D-X_A and DSPR1 depletion signals. A_i and B are the amplitudes and T_i and k are the time constants of the exponential components. τ is the amplitude-weighted lifetime extracted as $\tau = \sum_i A_i T_i / \sum_i A_i$.

Mode	2D-X_A		DSPR1	
Sample	2D	2D/Array	Array	2D/Array
B(%)	×	57	×	65
k(ps)	×	0.13	×	0.83
A_1(%)	52.9	20	64	×
T_1(ps)	0.50	2.7	1.06	×
A_2(%)	47.1	80	36	100
T_2(ps)	32.3	71.4	12.8	52.6
τ(ps)	15.4	57.7	5.3	52.6

The observed dynamics not only confirmed the indirect excitation of plasmonic modes of the Al array by the 2D-WS_2 excitons but also indicated that these excited plasmons had a feedback to the 2D-WS_2 excitons, affecting their dynamics, and increasing the amplitude-weighted lifetime of the 2D-X_A from ~15 ps to ~58 ps. Following energy transfer from 2D-WS_2 excitons to the Al metal array and excitation of its plasmons (see **Figure 5a**), the radiative

damping of these excited plasmons can lead to a dipole-dipole energy transfer back to the 2D-WS_2 semiconductor which increases the amplitude of its exciton depletion observed in **Figure 4a** and PL intensity enhancement observed in **Figure 1b**. Alternatively, during the entire ~ 100 ps lifetime of the 2D WS_2 excitons whereby the plasmonic nanodisks are excited, the hot-electrons generated through non-radiative Landau damping of these excited plasmons can tunnel to the conduction band of the 2D-WS_2 monolayer[22] as illustrated in **Figure 5b,** which also leads to an increase in the amplitude of the 2D-WS_2 exciton depletion observed in **Figure 4a.** We note that the hot-electron injected into the 2D-WS_2 monolayer at any given time-delay is the hot-electron resulting from Landau-damping of plasmons that were excited through energy transfer from 2D-WS_2 exciton a few tens of femtoseconds earlier. We note that based on energy band alignment shown in **Figure 5b**, hole transfer to the 2D-WS_2 is not possible. Since the time-constant of a decay is directly related to by how much the amplitude of the signal at any time-delay decreased compared to the initial amplitude, any increase in intensity at later time-delays or decrease in the initial amplitude leads to an increase of the time-constant of the exponential decay. For 2D-X_A exciton depletion dynamics in the hybrid sample, the initial amplitude is lower than that in the case of bare 2D-WS_2 semiconductor (because of energy transfer to the Al metal), and the amplitude at later time-delays is more than that in the case of bare 2D-WS_2 sample (because of energy and/or electron transfer from excited plasmons), consequently, the resulting decay dynamics are slower.

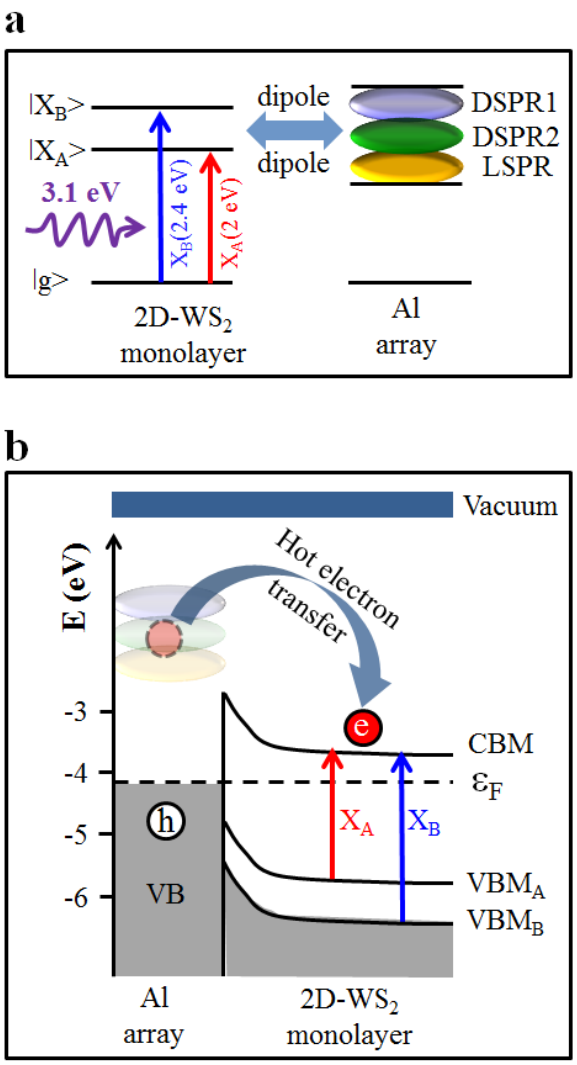

Figure 5. **a.** A schematic of the mechanism of energy transfer at the studied hybrid system. Following 3.1 eV excitation, which is off-resonance with respect to the Al array plasmonic modes but sufficient for the generation of 2D-WS_2 excitons, based on steady state absorption spectra shown in **Figure 2a**, energy transfer from the excited 2D-WS_2 excitons to the Al array can excite the metal plasmonic modes DSPR1, DSPR2, and LSPR through dipole-dipole interaction. $|g\rangle$ is the ground state of 2D-WS_2, and $|X_A\rangle$ and $|X_B\rangle$ are the excited excitons X_A and X_B, respectively. **b.** A schematic of the mechanism of charge transfer at the studied hybrid system. Following excitation of plasmons through energy transfer from 2D excitons as shown in **a**, the hot-electrons resulting from the non-radiative Landau-damping of excited plasmons are

injected into the conduction band of the 2D-WS_2 monolayer. Alternatively, the radiative relaxation of the excited plasmons leads to energy transfer back to the 2D excitons through dipole-dipole interaction as in **a**. The dotted horizontal line indicates the Al Fermi energy ε_F taken from [29]. VBM is the conduction band minimum and VBM_A and VBM_B are the valence band maxima resulting from spin-orbit split in the valence band of 2D-WS_2 monolayer taken from [30].

In summary, the ultrafast energy transfer between excitons generated in a 2D-WS_2 monolayer and plasmons in patterned Al nanodisk arrays were revealed by ultrafast pump probe dynamics. First, the selective excitation of excitons in the 2D WS_2 monolayer were shown to result in the production (after ~3 ps) of plasmons in the Al nanodisks that last as long (~100 ps) as the excitons in the 2D semiconductor. This extends the time that hot electrons are available for chemistry or charge transfer. Because the lifetime of excitons differs from one 2D semiconductor to another,[31] understanding this bidirectional energy transfer should allow the design of appropriate hybrid plasmonic/2D structures with the longest-lived exciton-excited plasmons for higher efficiencies in applications such as photodetectors, photovoltaics, and photocatalysis. Second, this plasmon re-excitation was shown to alter the dynamics of the 2D excitons compared to that within an unpatterned 2D crystal, decreasing absorption at the 2D-X_A and 2D-X_B exciton transitions at later time delays resulting from either dipole-dipole energy transfer or tunneling of hot-electrons to the conduction band of the 2D-WS_2 monolayer. These results may possibly help partially explain the increase in photoluminescence observed for plasmonic-enhanced TMD systems. The transfer of exciton energy to the metal nanodisks, followed by delayed re-excitation of the 2D TMD crystal, may serve to enhance the number of

photoexcited excitons that survive by bypassing fast (sub-ps) non-radiative exciton decay processes that were observed in **Figure 4a** in the absence of the plasmonic arrays.

METHODS

Sample preparation. 2D-WS_2 monolayers on SiO_2/Si substrates were prepared using chemical vapor deposition (CVD) as reported previously.[20,21] To pattern 2D-WS_2 crystals with aluminum plasmonic arrays, electron beam lithography (FEI DB-FIB with Raith pattern writing software) was used. Firstly, a layer of PMMA 495A4 was spin-coated on top of the Si/SiO_2 substrate with 2D-WS_2 crystals, followed by baking at 180^0C on a hot plate. In order to construct Al arrays of nanodisks with ~295 nm diameter, ~45 nm height, and spaced with ~420 nm pitch, a ~10 pA beam current was used for patterning. After pattern writing and developing, a 42 nm layer of Al was deposited using electron beam evaporation.

Time-resolved reflectance (TrR) measurements. A full description of the femtosecond pump-probe spectrometer (PPS) used in this work can be found in a our previous reports[20]. Briefly, the PPS is based on a titanium sapphire (Ti:Sa) oscillator (Micra, Coherent) with its output seeded by a Ti:Sa Coherent Legend (USP-HE) amplifier operating at 1 kHz repetition rate. The Legend amplifier provides pulses centered at 800 nm, with ~45 fs duration and 2.2 mJ energy per pulse. Pump pulses are the fundamental output of the Legend amplifier (1.55 eV) and its second harmonic at 3.1 eV. A small portion (~2 μJ) of the beam from the Legend amplifier was focused onto a 2-mm thick sapphire window to generate a white light continuum (WLC) probe, which covers a spectral region from 1.6 to 2.8 eV. At the sample, the pump and probe spot sizes were ~ 7 mm. The pump power was kept below 2 μJ/cm^2. A spectrograph (Shamrock 303i, Andor) coupled with a CCD (Andor Newton) equipped with an electron multiplier (EM) were used for detecting the reflected white light probe. At each time-delay, *t,* between the pump

and the probe, the percentage change in the reflectance contrast $\Delta R/R$ (%) was calculated as 100 x $(R_1-R_0)/R_0$, where R_1 and R_0 are the intensities of the reflected probe with pump on and off, respectively.

Numerical calculations. Numerical calculations of array absorbance were performed with CST Microwave Studio using a frequency domain solver. A domain of one particle was used, and periodic boundary conditions were imposed in both in-plane directions, thereby effectively modeling an infinite array. In the calculations, the array (permittivity data was taken from[32]) was placed on a 300-nm silicon dioxide substrate (permittivity data from[33]) followed by bulk silicon (permittivity data from[34]). Note that incidence light was normal to the surface for all the calculation.

ASSOCIATED CONTENT

Supporting Information

Additional analysis of transient absorption spectra at different time-delays and dynamics of the 2D-X_B exciton bleach.

AUTHOR INFORMATION

Corresponding Author

*E-mail: boulesbaaa@ornl.gov

Notes

The authors declare no competing financial interest.

ACKNOWLEDGMENTS

This research was conducted at the Center for Nanophase Materials Sciences, which is a DOE Office of Science User Facility. Synthesis of the two-dimensional materials was supported by the Materials Science and Engineering Division, Office of Basic Energy Sciences, U.S. Department of Energy. The authors thank Dr. Benjamin Lawrie from the Computational Sciences and Engineering Division at ORNL for the fruitful discussions.

REFERENCES

(1) Willets, K. A.; Van Duyne, R. P. Localized Surface Plasmon Resonance Spectroscopy and Sensing. *Annu. Rev. Phys. Chem.* **2007**, *58*, 267.

(2) Brongersma, M. L.; Halas, N. J.; Nordlander, P. Plasmon-induced hot carrier science and technology. *Nat. Nanotechnol.* **2015**, *10*, 25.

(3) Link, S.; El-Sayed, M. A. Optical Properties and Ultrafast Dynamics of Metallic Nanocrystals". *Annu. Rev. Phys. Chem.* **2003**, *54*, 331.

(4) Schuller, J. A.; Barnard, E. S.; Cai, W.; Chul Jun, Y.; White, J. S.; Brongersma, M. L. Plasmonics for extreme light concentration and manipulation. *Nat. Mater.* **2010**, *9*, 193.

(5) Clavero, C. Plasmon-induced hot-electron generation at nanoparticle/metal-oxide interfaces for photovoltaic and photocatalytic devices. *Nat. Photon.* **2014**, *8*, 95.

(6) Knight, M. W.; Sobhani, H.; Nordlander, P.; Halas, N. J. Photodetection with Active Optical Antennas. *Science* **2011**, *332*, 702.

(7) Christopher, P.; Xin, H.; Linic, S. Visible-light-enhanced catalytic oxidation reactions on plasmonic silver nanostructures. *Nat. Chem.* **2011**, *3*, 467.

(8) Atwater, H. A.; Polman, A. Plasmonics for improved photovoltaic devices. *Nat. Mater.* **2010**, *9*, 205.

(9) Mubeen, S.; Lee, J.; Singh, N.; Krämer, S.; Stucky, G. D.; Moskovits, M. An autonomous photosynthetic device in which all charge carriers derive from surface plasmons. *Nat. Nanotechnol.* **2013**, *8*, 247.

(10) Lawrie, B. J.; Evans, P. G.; Pooser, R. C. Extraordinary Optical Transmission of Multimode Quantum Correlations via Localized Surface Plasmons. *Phys. Rev. Lett.* **2013**, *110*, 156802.

(11) Mukherjee, S.; Libisch, F.; Large, N.; Neumann, O.; Brown, L. V.; Cheng, J.; Lassiter, J. B.; Carter, E. A.; Nordlander, P.; Halas, N. J. Hot Electrons Do the Impossible: Plasmon-Induced Dissociation of H_2 on Au. *Nano Lett.* **2013**, *13*, 240.

(12) Li, X.; Xiao, D.; Zhang, Z. Landau damping of quantum plasmons in metal nanostructures. *New J. Phys.* **2013**, *15*, 023011.

(13) Hartland, G. V. Optical Studies of Dynamics in Noble Metal Nanostructures. *Chem. Rev.* ***2011***, *111*, 3858.

(14) Zhang, X.; Chen, Y. L.; Liu, R. S.; Tsai, D. P. Plasmonic photocatalysis. *Rep. Prog. Phys.* **2013**, *76*, 046401.

(15) Lee, B.; Park, J.; Han, G. H.; Ee, H. S.; Naylor, C. H.; Liu, W.; Johnson, A. T. C.; Agarwal, R. Fano Resonance and Spectrally Modified Photoluminescence Enhancement in Monolayer MoS_2 Integrated with Plasmonic Nanoantenna Array. *Nano Lett.* **2015**, *15*, 3646.

(16) Butun, S.; Tongay, S.; Aydin, K. Enhanced Light Emission from Large-Area Monolayer MoS_2 Using Plasmonic Nanodisc Arrays. *Nano Lett.* **2015**, *15*, 2700.

(17) Najmaei, S.; Mlayah, A.; Arbouet, A.; Girard, C.; Léotin, J.; Jun Lou, J. Plasmonic Pumping of Excitonic Photoluminescence in Hybrid MoS_2-Au Nanostructures. *ACS Nano* **2014**, *12*, 12682.

(18) Lee, K. C. J.; Chen, Y. H.; Lin, H. Y.; Cheng, C. C.; Chen, P. Y.; Wu, T. Y.; Shih, M. H.; Wei, K. H.; Li, L. J.; Chang, C. W. Plasmonic Gold Nanorods Coverage Influence on Enhancement of the Photoluminescence of Two-Dimensional MoS_2 Monolayer. *Sci. Rep.* **2015**, *5*, 16374.

(19) Inouye, H.; Tanaka, K.; Tanahashi, I.; Hirao, K. Ultrafast dynamics of nonequilibrium electrons in a gold nanoparticle system. *Phys. Rev. B* **1998**, *57*, 11334.

(20) Boulesbaa, A.; Huang, B.; Wang, K.; Lin, M. W.; Mahjouri-Samani, M.; Rouleau, C.; Xiao, K.; Yoon, M.; Sumpter, B.; Puretzky, A.; Geohegan, D. Observation of two distinct negative trions in tungsten disulfide monolayers. *Phys. Rev. B* **2015**, *92*, 115443.

(21) Wang, K.; Huang, B.; Tian, M.; Ceballos, F.; Lin, M. W.; Mahjouri-Samani, M.; Boulesbaa, A.; Puretzky, A. A.; Rouleau, C. M.; Yoon, M.; Zhao, H.; Xiao, K.; Duscher, G.; Geohegan, D. B. Interlayer Coupling in Twisted WSe_2/WS_2 Bilayer Heterostructures Revealed by Optical Spectroscopy. *ACS Nano* **2016**, *10*, 6612.

(22) Lin, H. Y.; Cheng, C. L.; Chou, Y. Y.; Huang, L. L.; Chen, Y. F. Enhancement of band gap emission stimulated by defect loss. *Opt. Express* **2006**, *14*, 2372.

(23) Shin, T.; Cho, K. S.; Yun, D. J.; Kim, J.; Li, X. S.; Moon, E. S.; Baik, C. W.; Kim, S. I.; Kim, M.; Choi, J. H.; Park, G. S.; Shin, J. K.; Hwang, S.; Jung, T. S. Exciton Recombination, Energy-, and Charge Transfer in Single- and Multilayer Quantum-Dot Films on Silver Plasmonic Resonators. *Sci. Rep.* **2016**, *6*, 26204.

(24) Cui, Q.; Ceballos, F.; Kumar, N.; Zhao, H. Transient Absorption Microscopy of Monolayer and Bulk WSe_2. *ACS Nano* **2014**, *8*, 2970.

(25) Zhou, W.; Hua, Y.; Huntington, M. D.; Odom, T. W. Delocalized Lattice Plasmon Resonances Show Dispersive Quality Factors. *J. Phys. Chem. Lett.* **2012**, *3*, 1381.

(26) Moody, G.; Schaibley, J.; Xu, X. Exciton dynamics in monolayer transition metal dichalcogenides. *J. Opt. Soc. Am.* **2016**, *33*, c39.

(27) Wang, H.; Zhang, C.; Rana, F. Ultrafast Dynamics of Defect-Assisted Electron−Hole Recombination in Monolayer MoS2. *Nano Lett.* **2015**, *15*, 339.

(28) He, J.; He, D.; Wang, Y.; Cui, Q.; Ceballos, F.; Zhao, H. Spatiotemporal dynamics of excitons in monolayer and bulk WS2. *Nanoscale* **2015**, *7*, 9526.

(29) Eastment, R. M.; Mee, C. H. B. Work function measurements on (100), (110) and (111) surfaces of aluminium. *J. Phys. F* **1973**, *3*, 1738.

(30) Gong, C.; Zhang, H.; Wang, W.; Colombo, L.; Wallace, R. M.; Cho, K. Band alignment of two-dimensional transition metal dichalcogenides: Application in tunnel field effect transistors. *Appl. Phys. Lett.* **2013**, *103*, 053513.

(31) Palummo, M.; Bernardi, M.; Grossman, J. C. Exciton Radiative Lifetimes in Two-Dimensional Transition Metal Dichalcogenides. *Nano Lett.* **2015**, *15*, 2794−2800.

(32) Palik, E. D. *Handbook of Optical Constant of Solids I*; *Academic Press*: New York, 1**985**, pp 369-406.

(33) Gao, L.; Lemarchand, F.; Lequime, M. Refractive index determination of SiO_2 layer in the UV/Vis/NIR range: spectrophotometric reverse engineering on single and bi-layer designs. *J. Eur. Opt. Soc.Rapid.* **2013**, *8*, 13010.

(34) Palik, E. D. *Handbook of Optical Constant of Solids I*; *Academic Press*: New York, 1**985**, pp 547-569.

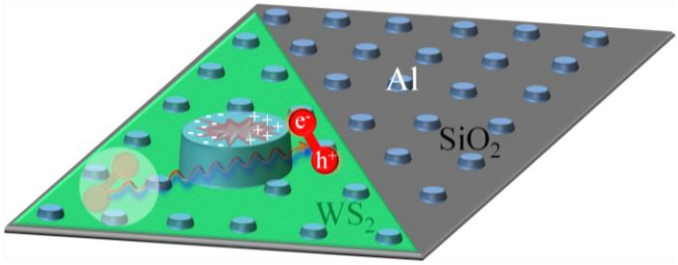

TOC

Ultrafast Dynamics of Metal Plasmons Induced by 2D Semiconductor Excitons in Hybrid Nanostructure Arrays

Abdelaziz Boulesbaa, Viktoriia E. Babicheva, Kai Wang, Ivan I. Kravchenko, Ming-Wei Lin, Masoud Mahjouri-Samani, Christopher Jacob, Alexander A. Puretzky, Kai Xiao, Ilia Ivanov, Christopher M. Rouleau, and David B. Geohegan

An array of aluminum disks is printed on a 2D-WS_2 monolayer which is supported on an Si/SiO_2 substrate. Following photoexcitation of the 2D-WS_2 monolayer and generation of excitons, while these excited excitons diffuse through the heterostructure, they transfer energy to the Al array and excite its plasmons. It is found that the plasmons or subsequently the resulting hot-electrons stay excited as long as the 2D-WS_2 excitons live. These results open new opportunities for plasmonics based devices where long-lived plasmons and hot electrons are indisponsable for the performance effeciency of the optoelectronic device.